

# Journal of Geophysical Research: Atmospheres

## RESEARCH ARTICLE

10.1002/2015JD023299

**Key Points:**

- Sonde-measured Costa Rican O<sub>3</sub> and H<sub>2</sub>O vapor show distinct seasonal variations
- Water vapor is too low for the air to be locally dehydrated
- Three processes lead to tracer variability: waves, path changes, and sources

**Correspondence to:**M. R. Schoeberl,  
mark.schoeberl@mac.com**Citation:**Schoeberl, M. R., H. B. Selkirk, H. Vömel, and A. R. Douglass (2015), Sources of seasonal variability in tropical upper troposphere and lower stratosphere water vapor and ozone: Inferences from the Ticosonde data set at Costa Rica, *J. Geophys. Res. Atmos.*, 120, 9684–9701, doi:10.1002/2015JD023299.

Received 24 FEB 2015

Accepted 20 JUL 2015

Accepted article online 22 JUL 2015

Published online 17 SEP 2015

## Sources of seasonal variability in tropical upper troposphere and lower stratosphere water vapor and ozone: Inferences from the Ticosonde data set at Costa Rica

Mark R. Schoeberl<sup>1</sup>, Henry B. Selkirk<sup>2</sup>, Holger Vömel<sup>3</sup>, and Anne R. Douglass<sup>4</sup><sup>1</sup>Science and Technology Corporation, Columbia, Maryland, USA, <sup>2</sup>GESTAR/NASA GSFC, Greenbelt, Maryland, USA, <sup>3</sup>NCAR Earth Observations Laboratory, Boulder, Colorado, USA, <sup>4</sup>NASA GSFC, Greenbelt, Maryland, USA

**Abstract** We present an analysis of joint balloonsonde profiles of water vapor and ozone made at Costa Rica from 2005 to 2011 using compositing techniques, tracer-tracer diagrams, and back trajectory methods. Our analysis reveals important seasonal differences in structure in the upper troposphere and lower stratosphere. Water vapor amounts in boreal winter at Costa Rica are much lower than expected from local ice saturation temperatures. The boreal summer data show both higher average water vapor amounts and a much higher level of variability than the winter data. To understand this seasonal contrast, we consider three sources of tracer variability: wave-induced vertical motion across strong vertical gradients (“wave variability”), differences in source air masses resulting from horizontal transport (“source variability”), and changes induced along parcel paths due to physical processes (“path variability”). The winter and summer seasons show different mixes of these three sources of variability with more air originating in the tropical western Pacific during winter.

### 1. Introduction

It has long been recognized that the dehydration processes near the tropical tropopause [see, e.g., Randel and Jensen, 2013; Jensen et al., 2013] play a pivotal role in regulating the amount of water vapor that enters the stratosphere. The fine-scale dynamical processes associated with dehydration are difficult to diagnose in the remote regions of the tropical tropopause, and the occurrence of supersaturated regions both within and outside of clouds is a puzzle [Peter et al., 2006]. Trajectory models based on reanalysis fields [e.g., Schoeberl et al., 2012; Schoeberl and Dessler, 2011; Fueglistaler et al., 2005.] have had considerable success simulating the net flow of water vapor into the stratosphere and even its regional and seasonal variations. These models rely on simple parameterizations of dehydration, leaving large uncertainties on the relative roles of three, often compensating, dynamical processes that set the stage for dehydration: large-scale transport [Newell and Gould-Stewart, 1981; Holton and Gettelman, 2001], convective overshooting [Danielsen, 1982; Sherwood and Dessler, 2003], and gravity waves [Jensen and Pfister, 2004]. Reducing these uncertainties is required to improve the representation of stratosphere-troposphere exchange and dehydration in the atmospheric general circulation models that lie at the core of climate models. Such improvements are necessary if we are to understand long-term trends of water vapor in the upper troposphere and lower stratosphere (UT/LS).

Balloonsonde and aircraft observations of ozone and water vapor in the tropical UT/LS reveal fine-scale features that are below the vertical resolution of satellite sounding systems. For example, the layers of ice supersaturation commonly observed in tropical frostpoint hygrometer balloon soundings and aircraft data [Vömel et al., 2002; Krämer et al., 2009; Selkirk et al., 2010] are generally too shallow to be seen by the Microwave Limb Sounder (MLS) instrument. To the extent that such fine-scale structures are the fingerprint of processes that influence UT/LS composition, an understanding of how these processes contribute to the observed structure can lead to a better interpretation of the lower vertical resolution information provided by satellite instruments and thus more realistic modeling of the UT/LS water vapor budget. Because of its long lifetime in the UT/LS, ozone is essentially a passive tracer. Thus, ozone measurements can be used along with the accompanying temperature and wind measurements to help identify the dynamical processes that produced these fine-scale structures.

Consider, for example, the effects of gravity waves in deep convective zones. The temperature perturbations associated with these waves introduce a degree of variability in the local cold point (CP) [Selkirk et al., 2010]. As a result, incremental dehydration can occur at any level at which the temperature deviations are large

**Table 1.** Modes of Nonlocal Variability in the UT/LS

	High Ozone ( $\geq 100$ ppbv)	Low Ozone ( $\leq 100$ ppbv)
High water vapor ( $\geq 5$ ppmv)	Convective hydration of midlatitude stratospheric air parcels (path)	Tropical upper troposphere, outside tropical West Pacific (TWP) (source)
Low water vapor ( $\leq 5$ ppmv)	Tropical stratosphere (source)	Upper troposphere, tropical West Pacific (TWP) (source)

enough to drive the background water vapor into supersaturation. However, the existence of supersaturated air does not imply dehydration nor cloud formation as supersaturated air without ice crystals is widely observed in the tropics [Jensen *et al.*, 2013]. Selkirk *et al.* [2010] argue that in the deep convective environment of Costa Rica during boreal summer, gravity waves induce an enhanced frequency of supersaturation and dehydration events between 360 K and 380 K. They termed this layer of active dehydration as the “tropopause saturation layer” to distinguish it from the deeper tropical tropopause layer in which it is embedded.

We call the tracer variability due to gravity waves “wave variability.” This type of variability can be inferred in a sounding assuming that the motion is adiabatic. A trace gas perturbation  $\mu'$  is approximately determined by

$$\mu' = \theta' \bar{\mu}_z / \bar{\theta} \quad (1)$$

where  $\theta$  is the potential temperature,  $\mu$  is the trace gas mixing ratio, the subscript  $z$  indicates vertical derivative, prime indicates a perturbation, and the overbar indicates a mean profile.

There are two possible modes of nonlocal variability that can be identified in analysis of balloonsondes. The first mode, which we call “source variability,” arises from large-scale transport processes. For example, it is well known that in spring, the concentration of ozone along the 360 K isentropic surface varies significantly between the tropics and midlatitudes [e.g., Pan *et al.*, 2004]. This variation is due to descent of ozone from the midlatitude stratosphere. Mixing between the midlatitudes and the tropics will bring dry, high-ozone midlatitude stratospheric air into the tropical upper troposphere. In contrast, air from the tropical western Pacific (TWP) upper troposphere (UT) may also be quite dry but have very low ozone mixing ratios. As filaments of air from the TWP UT sweep over the Ticosonde balloonsonde site in Costa Rica, for example, the profile will show layers, sometimes quite shallow, with water vapor and ozone characteristics very different from air in the rest of the profile. Such layers are evidence of source variability. In an even broader context, differences between Southern Hemisphere and Northern Hemisphere tropical ozone soundings can be attributed to the differences in transport into the tropics between the two hemispheres; such transport differences are clearly evident in the ozone annual cycle at the tropical tropopause [Randel *et al.*, 2007; Stolarski *et al.*, 2014].

The second remote mode of variability we call “path variability.” It arises from changes in the water concentration by dehydration or by the convective injection of ice along the parcel’s path between its source region and balloon site. For example, a high-ozone midlatitude air parcel with low water vapor may pass over a convective system where ice detrainment increases the water vapor. This parcel may then become a high-ozone, high-water mixing ratio parcel (see Table 1). Such parcels have been observed in the North American monsoon [Anderson *et al.*, 2012].

Table 1 summarizes some different combinations of water vapor and ozone anomalies in the UT/LS and their relation to the two different modes of nonlocal variability as they influence the composition of air over Costa Rica.

In this paper, we examine the contributions of these two modes of nonlocal variability and local wave variability to the vertical structure of water vapor and ozone soundings at Costa Rica. These water vapor and ozone soundings have been made at three closely located sites near San José since 2005 as part of the Ticosonde project [Selkirk *et al.*, 2010; Fujiwara *et al.*, 2010; Pan *et al.*, 2014]; in this paper we have used the soundings through the end of 2011. These data include both monthly launches of water vapor/ozone balloonsondes and intensive observations from four multiweek campaigns between 2005 and 2007; three of these accompanied NASA airborne campaigns.

We will show with scatter diagrams of water vapor and ozone mixing ratios from the balloon soundings that there are significant seasonal differences in the contributions from wave, source, and path variability. We augment the analysis by comparing the variance in the balloon soundings to simulated profiles constructed from water vapor and ozone data from the Aura Microwave Limb Sounder (MLS) using a new reverse domain filling technique.

**Table 2.** Ticosonde Launch Sites<sup>a</sup>

Site	Latitude, longitude, elevation	Dates	Intensive Observation Periods
A. Juan Santamaria International AP, Alajuela	9.99°N, 84.22°W, 0.9 km	8 Jul 2005 to 28 Sep 2005 (25) 2 May 2007 to 22 Dec 2009 (48)	TCSP: 8–25 Jul 2005 (23) TC4: 16 Jul to 9 Aug 2007 (14)
B. Universidad Nacional, Heredia	10.00°N, 84.11°W, 1.2 km	18 Oct 2005 to 10 Jan 2007 (53) 9 Jan 2010 to 16 Feb 2011 (12)	CR-AVE: 4 Jan to 23 Feb 2006 (27) Veranillo: 5–31 Jul 2006 (15)
C. Universidad de Costa Rica, San Pedro	9.94°N, 84.04°N, 1.2 km	5 Mar 2011 to 9 Dec 2011 (5)	

<sup>a</sup>The total number of CFH water vapor profiles is given in parentheses.

In section 2 we describe the observations and our screening to produce a seasonally compositized Ticosonde data set. In section 3 we start our analysis by examining the contributions of adiabatic wave motions of ozone variability. We then analyze a composite data set as a function of potential temperature. In section 4 we explore the seasonally varying relationships between water vapor and ozone using both scatter diagrams and simulated profiles from MLS. Variations in the data can be attributed to various source regions or the addition of water by convection. Back trajectories from San José, Costa Rica, for summer and winter provide insights into the sources of air observed by the balloonsondes. Discussion and conclusion sections follow these analysis sections. Our results are discussed further in section 5 and summarized in section 6.

## 2. Observations

We examine the behavior of ozone and water vapor in the UT/LS in our Costa Rica balloonsonde data set in two seasons: boreal winter (November–March) and summer (June–July–August, JJA). We then compare the sonde data to water vapor and ozone data from the MLS measurements over Costa Rica.

### 2.1. Sounding Data

Since July 2005 water vapor–ozone and ozone soundings have been conducted in Costa Rica by the Ticosonde project; these observations are ongoing. The Ticosonde data may be obtained from the Aura Validation Data Center (AVDC, <http://avdc.gsfc.nasa.gov>). In this study we analyze the soundings taken through December 2011. During this period, launches were made from three sites in the greater San José region: (A) Juan Santamaria International Airport in Alajuela, (B) the Universidad Nacional in Heredia, and (C) the Universidad de Costa Rica in San Pedro. These sites are located no more than 21 km apart. Table 2 lists the three locations and the number of soundings that were launched from each along with the total number of balloonsondes measuring water vapor.

Water vapor is measured with the Cryogenic Frostpoint Hygrometer (CFH) [Vömel *et al.*, 2007], a lightweight (400 g) instrument operating on the chilled-mirror principle. Ozone is measured with the electrochemical concentration cell ozonesonde [Komhyr *et al.*, 1995]. Each balloonsonde payload is equipped with a radiosonde to measure temperature, pressure, and relative humidity and to provide telemetry. Up to mid-April 2010, this was the Vaisala RS80 radiosonde, and winds were obtained through a Garmin GPS installed in the lid of the ozonesonde. Subsequent CFH launches have employed the Intermet iMet-1-RS, a GPS radiosonde.

CFH data are routinely checked postflight to remove gross instrumental artifacts [Vömel *et al.*, 2007]. The data used in this study were further postprocessed to reduce the uncertainty in the frostpoint temperature due to instrument controller instabilities. This is the largest source of frostpoint hygrometer measurement uncertainty and has been estimated at 0.5°C; all other sources of uncertainty are < 0.11°C [Vömel *et al.*, 2007]. In the postprocessing, the raw data were passed through a low-pass filter in the time domain with a cutoff frequency varying as a function of the frostpoint temperature. The processed sondes were then screened to remove soundings that did not provide ozone and frostpoint temperatures to at least 380 K potential temperature; only ascent data are considered because descent data are considered unreliable.

### 2.2. MLS Data

We include in the analysis water vapor and ozone version 3.3 data from the Aura Microwave Limb Sounder (Jet Propulsion Laboratory (2011), Earth Observing System Aura Microwave Limb Sounder (MLS) version

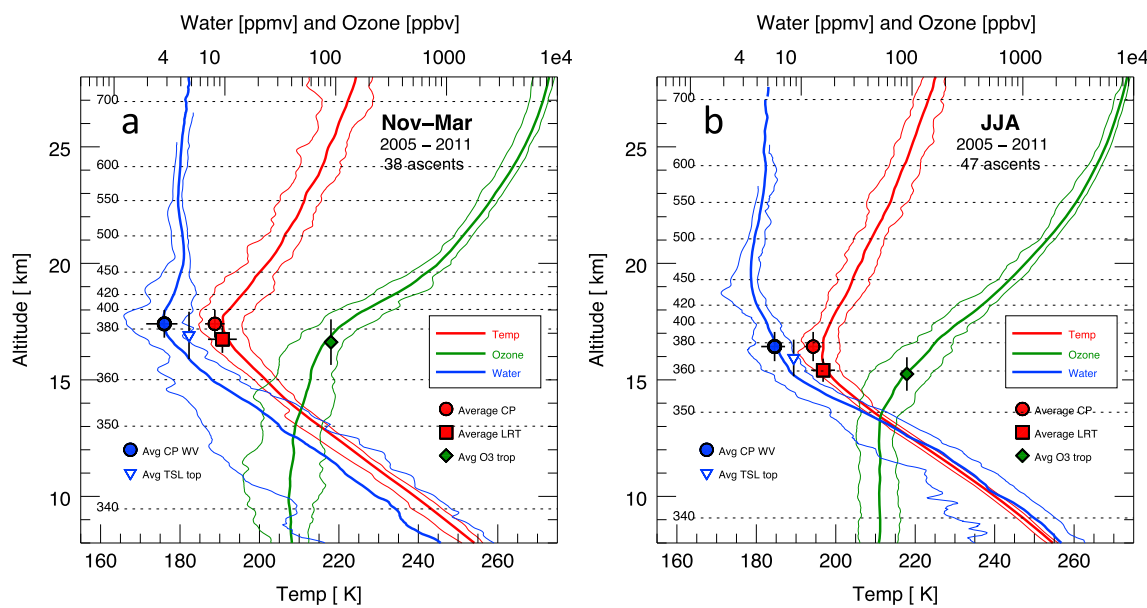


**Figure 1.** Long-term mean UT/LS profiles for boreal (a) winter (November–March) and (b) summer (June–August) of temperature (red), ozone mixing ratio (green), and water vapor mixing ratio (blue), 2005–2011. Lighter lines denote the 5th and 95th percentiles of the respective samples at each 10 m averaging level. The average CP and LRT temperatures and altitudes are shown as red filled circles and squares, respectively; error bars denote  $\pm 1$  standard deviation. The mean and standard deviation of the CP water vapor mixing ratio are shown with the blue filled circle. The mean position and standard deviation of the ozone tropopause (see text) are indicated by the green diamond with vertical bars. Finally, the blue inverted triangle shows the mean water vapor mixing ratio and altitude of the highest point of saturation in each profile and its standard deviation in altitude. All profiles smoothed with 21-point running-mean filter before plotting.

3.3 level 2 data quality and description document, JPL D-33509). These data were averaged over the 5 years 2005–2010, approximately the same period as the sounding data here. The MLS data were first interpolated to  $10^{\circ}\text{N}$ ,  $84^{\circ}\text{W}$ , which is within  $0.2^{\circ}$  of the location of each of the three Costa Rican sites, and then this MLS profile was interpolated onto the 72-level Modern-Era Retrospective Analysis for Research and Applications (MERRA) [Rienecker *et al.*, 2011] vertical grid.

### 3. Analysis of Observations

In the sections below we discuss the Ticosonde and MLS observations.

#### 3.1. Modes of Variability in Temperature, Ozone, and Water Vapor: Height Coordinates

We begin with an examination of the mean structure in height coordinates of temperature, ozone, and water vapor in the winter and summer seasons in the 2005–2011 period. We first interpolated the ascent portions of each sounding to a 10 m vertical grid and calculated averages and standard deviations on that grid. Soundings with unrealistic temperatures or ozone values were discarded and the statistics recomputed as necessary. The final quality-controlled and screened data set contained 38 soundings for the November–March season and 47 soundings in the June–August season.

Figure 1 shows average profiles of temperature and the mixing ratios of ozone and water vapor for the two seasons. To show the variability in the respective quantities, we have added profiles of the 5th and 95th percentile observations. On the temperature profiles the mean cold point (CP) and lapse rate tropopause (LRT) are plotted in red symbols with vertical and horizontal bars equal to 1 standard deviation in height and temperature, respectively. The mean height and standard deviation of the chemical or ozone tropopause, here defined as  $[O_3] = 90 \text{ ppbv}$  [Prather *et al.*, 2011], are plotted on the ozone profile. The CP is also plotted on the water vapor profile in blue. Finally, we show the mean water vapor mixing ratio of the highest saturated point in each profile at its mean height, with bars representing the standard deviation of the altitude. The latter corresponds to the upper boundary of the Tropopause Saturation Layer or TSL [Selkirk *et al.*, 2010]. Table 3 summarizes the long-term seasonal mean heights for the CP, the LRT, the ozone tropopause, and the TSL upper boundary. To increase the sample size, we extend the “winter” domain to include measurements made in November and March.

**Table 3.** Long-Term Means for November–March and June–August for Various Quantities Defined at the CP Tropopause, the Top of the Tropopause Saturation Layer, the LP Tropopause, and the Ozone Tropopause<sup>a</sup>

	Altitude (km)		Temperature (K)		Potential Temperature (K)		O <sub>3</sub> (ppbv)		H <sub>2</sub> O (ppmv)	
	Nov–Mar	JJA	Nov–Mar	JJA	Nov–Mar	JJA	Nov–Mar	JJA	Nov–Mar	JJA
CP tropopause	17.4 (37)	16.4 (47)	188.8 (37)	194.3 (47)	380.3 (37)	372.4 (47)	107 (37)	137 (47)	2.84 (36)	5.75 (47)
Top of TSL	16.9 (26)	15.9 (43)	190.3 (26)	196 (43)	374.1 (26)	366.6 (43)	87.6 (26)	121 (43)	4.75 (26)	8.55 (43)
LP tropopause	16.7 (37)	15.4 (47)	190.7 (37)	196.8 (47)	371.3 (37)	358.5 (47)	76.3 (37)	86.0 (47)	3.44 (36)	7.83 (47)
Ozone tropopause	16.6 (36)	15.3 (45)	193.9 (36)	199.2 (45)	375.3 (36)	360.1 (45)			3.55 (34)	10.0 (44)

<sup>a</sup>Sample sizes in parentheses.

Figure 1 reveals a number of important differences in the structure of the UT/LS between winter and summer. First, while the temperatures in both seasons are roughly the same at 25 km, below this level the winter temperature profile is substantially colder than in summer (i.e., temperatures are 8 K cooler at 18 km, the mean CP is 5.5 K colder, and it lies 7.9 K higher in potential temperature in winter than summer). Thus, the vertical temperature gradient in lowermost stratosphere in winter must be steeper than in summer. A similar pattern holds for the ozone gradient. Everywhere below ~700 K, ozone is lower in winter than in summer, and the ozone tropopause is higher. This is manifested in a much stronger vertical ozone gradient in winter, particularly below 20 km (~460 K) where there is a noticeable inflection point in the ozone profile. In contrast, the most interesting feature of the mean summer ozone profile is in the upper troposphere, where a near-constant profile at ~50 ppbv rapidly gives way at 350 K to a vertical gradient. The relatively sharp transition in the summer ozone profile bears some resemblance to the mean profile discussed by *Folkins et al.* [1999], but in winter, the upper tropospheric ozone increase is less pronounced.

An important similarity between the two seasons is in the location of the CP. In the mean it is located above the mean position of the ozone tropopause and thus is, on average, in the stratosphere, though barely so as Table 3 indicates. The table also indicates that saturation does occur well above the ozone tropopause.

The other notable differences between the winter and summer mean profiles are in water vapor. In winter, the average profile reaches a minimum of 2.7 ppmv at 17.5 km (386 K potential temperature)—very close to the average CP. It then increases to 4.3 ppmv at 20.5 km followed by a secondary minimum of ~3.8 ppmv at ~23 km. In summer, the profile minimum of 3.5 ppmv near 19.8 km (464 K) lies well above the mean CP. These features are elements of the global-scale water vapor tape recorder [*Mote et al.*, 1996]. That is, the low water vapor values from previous winter can be seen to have moved upward with the tropical upwelling circulation.

The similarities and differences between the seasonal mean UT/LS structure provide the context to consider the vertical distribution of temporal variability in the two seasons. Here we infer the latter from the spread between the 5th and 95th percentile observations profiled in Figure 1. In both seasons, the temperature range is relatively constant in the upper troposphere up to the 350–355 K potential temperature levels. Above this level the variability of temperature increases, markedly so in the summer season where the 8 K range at 15 km is more than double the range at 10 km. A similar doubling in the range of ozone mixing ratios is also seen over this same altitude range during summer. The temperature range in summer widens further above the mean position of the ozone tropopause at 360 K.

In contrast to the increases in temperature and ozone variability near the 355 K potential temperature level, both seasons show a narrowing of the range of water vapor variability above this level and then a local maximum in range near the level of the mean CP. The latter is more pronounced in the winter season. In the lower stratosphere, both seasons show a reduction in variability, and in summer most of the narrowing of the water vapor mixing ratio variability occurs in conjunction with the upper boundary of the TSL at ~17.2 km and 386 K, decreasing by half. Here also the temperature range narrows as well. In the winter profile, the narrowing happens more gradually and reaches a steady stratospheric value only above 20 km and 460 K. Unlike the summer, this reduction in variability is not associated with clear features in the variability of either temperature or ozone.

The analysis so far suggests that ozone variability in the UT/LS is coupled to temperature variability above the 350–355 K level and the vertical motions driving the latter. In summer this is evident both in the change

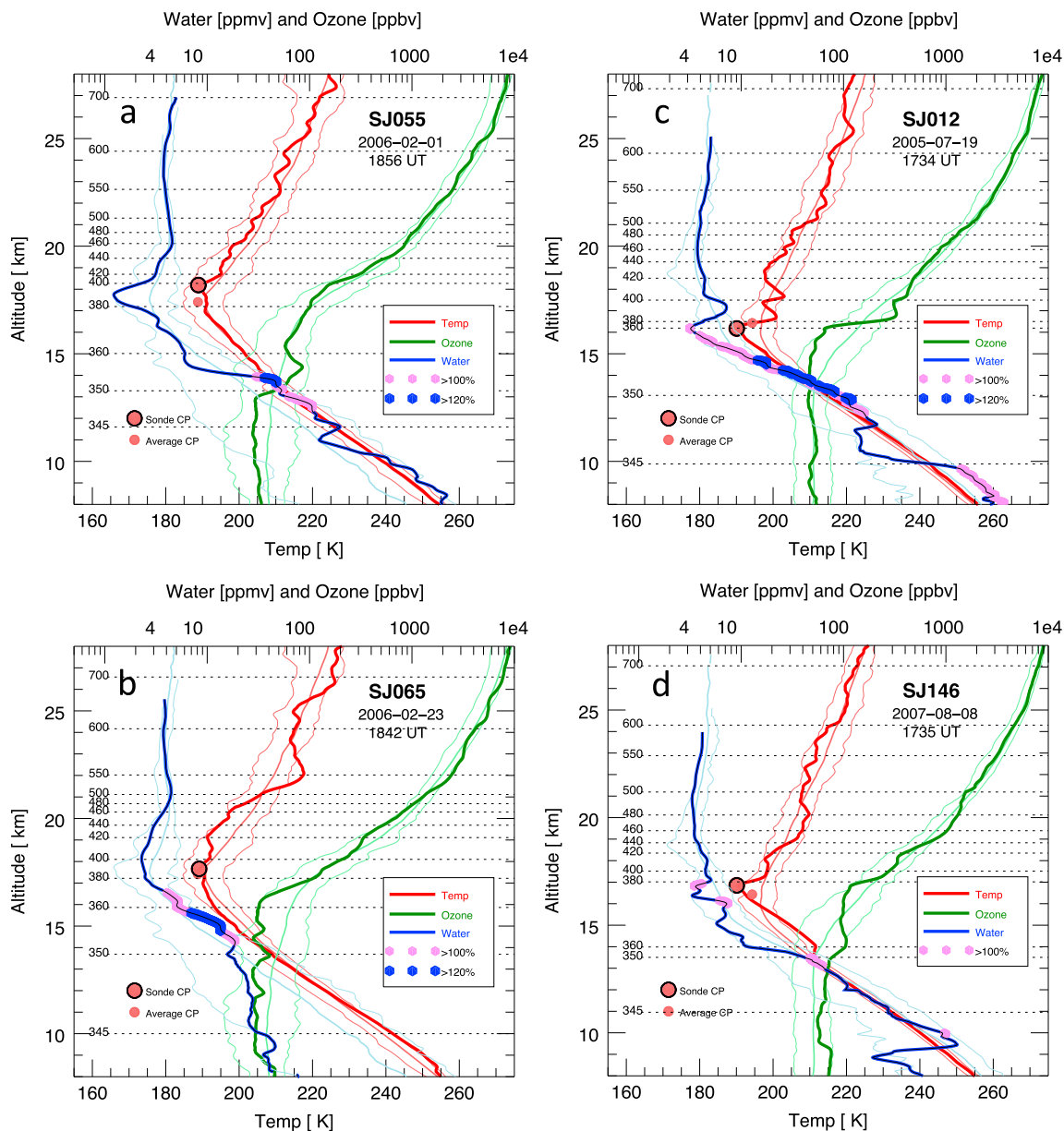


**Figure 2.** Selected UT/LS profiles from the boreal (a, b) winter season and (c, d) summer season; water vapor in blue, temperature in red, and ozone in green as in Figure 1. Lighter lines denote the corresponding long-term seasonal average profiles and envelopes of 5th and 95th percentiles for each profile. The CP and its long-term seasonal average are shown as with large red-filled circle and a smaller red dot, respectively. Layers of saturation of the water vapor profiles are shown with large cyan and blue circles, the latter for supersaturations greater than 20%. All profiles smoothed with a 21-point running-mean filter.

of the ozone gradient at 350 K and in the increase of variability at that level in both quantities. These features are less well defined in winter, but the upward shift of the thermal tropopause is matched by a similar increase of the ozone tropopause altitude. Similar inferences cannot be made with respect to the variability of water vapor given its more complicated vertical structure and the fact that it is not conserved under freezing and sublimation.

To gain a more complete picture of the interrelationships between anomalies of temperature, ozone mixing ratio, and water vapor mixing ratio, we selected two soundings each from winter and summer seasons that had strong ozone anomalies in the upper troposphere, lower stratosphere, or both. The two winter season soundings selected were SJ055 and SJ065. The two summer season selected were SJ012 and SJ146. These are plotted in Figure 2 and discussed below.

*SJ055* (1 February 2006, Figure 2a) has two layers of prominent water vapor anomalies. First, just above the lapse rate tropopause at 17 km, there is a near-isothermal layer of extremely low water vapor values (down to 1 ppmv) extending to the CP at ~400 K. The second is a layering of anticorrelated water vapor and ozone anomalies between 11 and 15 km with a saturation layer at its core. The corresponding temperature anomalies are very weak due to the roughly moist adiabatic mean lapse rate. Anomalies in the lower layer are consistent with wave-driven adiabatic vertical motion, while the lack of ozone anomalies and near-normal temperatures accompanying the low water vapor values above the CP tropopause suggests horizontal transport from a remote tropical source.

In *SJ065* (23 February 2006, Figure 2b) there are three layers of alternating temperature anomalies above 18 km shown in the figure, and this deep wave structure is broadly reflected in the anomaly patterns in water vapor and ozone. The most significant features are (i) a saturated layer below the CP with low (<40 ppbv) ozone, (ii) low water vapor in the lower stratosphere up to 480 K, and (iii) strong positive temperature anomalies above that level with high ozone but no significant water vapor anomalies. The latter are consistent with the very weak mean water vapor gradient above ~500 K in this season while the negative anomalies in water in (ii) are in line with the stronger mean gradient in the lowermost stratosphere in this season.

*SJ012* (19 July 2005, Figure 2c) is distinguished by a very deep layer of supersaturation extending from 12 km to a CP at ~360 K just above 16 km. In the last kilometer of this layer, the anomalously cold temperatures are forcing dehydration, and at the CP the water vapor is driven down to 3 ppmv, less than half of the seasonal average. It is evident that adiabatic ascent is driving this dehydration from the low (<50 ppbv) and near-constant ozone to within several hundred meters of the CP. The second notable feature of this sounding is the strong positive water vapor anomaly above the CP and in the stratosphere. It peaks at 8 ppmv at 390 K and just above 17 km. This high water vapor lies in an adiabatic layer with ozone values of ~300 ppbv. While the ozone values are consistent with descent of ~1 km down the mean vertical gradient, the water vapor values are not, and one possibility is that this high-water and high-ozone layer had been advected into the tropics from higher latitudes. Indeed, back trajectory calculations (not shown) indicate that this is the case for this layer.

*SJ146* (8 August 2007, Figure 2d) is from the NASA TC4 campaign and may be another example of transport from higher latitudes. However, this sounding has a pronounced kink in temperature or false tropopause beginning at 350 K with a near-isentropic layer above 360 K extending up to the CP close to 380 K. This 3 km deep layer has nearly constant ozone, consistent with adiabatic ascent. However, if this ascent were local, the ozone values in the layer would have been several tens of parts per billion by volume lower than the ~100 ppbv observed in the layer. Likewise, the water vapor is very low through most of the layer, reaching 3 ppmv at 16.4 km. This layer may thus be an example of a layer transported into the region. The soundings on days immediately preceding and after all displayed the same kink in the temperature, so this feature was persistent and likely relatively large in scale.

In summary, we see a tendency for an inverse relationship between temperature and ozone anomalies, especially in the lower stratosphere where the mean seasonal gradients are extremely strong. This is clear evidence of adiabatic motions generating ozone anomalies through the movement of parcels up and down the mean ozone gradient. There are also indications of horizontal transport: the layer of very low water vapor at tropopause level in *SJ065* (Figure 2b) and the layer of 100 ppbv ozone in *SJ146* (Figure 2d). Depending upon the origin of the transported air, this transport may carry with it water vapor anomalies. We will argue below that layers of high water vapor and high ozone such as observed just above the tropopause in *SJ012* (Figure 2c) are likely to be examples of air parcel transport from higher latitudes that have not encountered temperatures cold enough to alter the water vapor concentration, that is, "source" variability. In contrast, low water vapor anomalies near the tropopause such as in *SJ065* may be examples of either source or "path" variability.

A quantitative estimate of the role of adiabatic motions to the ozone variance can be obtained by calculating the fractional contribution of adiabatic motion to the change in ozone through adiabatic motion from (1), viz.,

$$F_\theta = (\bar{V}_z / \bar{\theta}_z) V_\theta / V_\mu \quad (2)$$

where  $V_\theta$  and  $V_\mu$  are the variances of potential temperature and the mixing ratio, respectively. We calculated  $F_\theta$  for ozone as the fraction of total variability for both the November–March period and the June–August period.

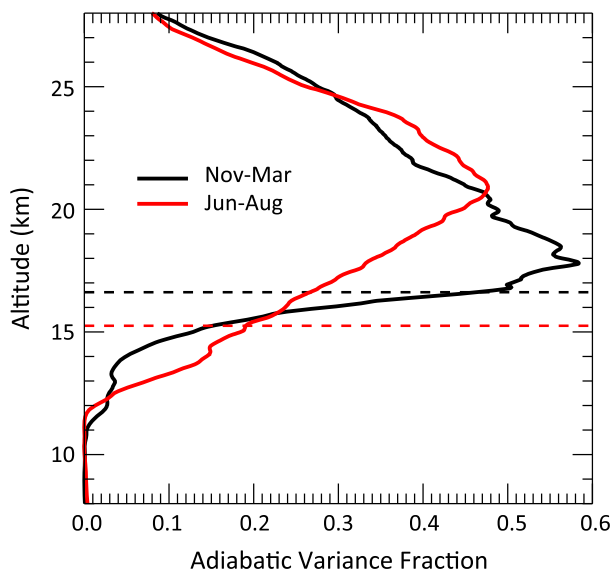


**Figure 3.** Fraction of the total variance of ozone mixing ratio due to adiabatic motion (see text) for the boreal winter season (black) and summer (red). Dashed lines indicate position of ozone tropopause. Profiles smoothed with a 21-point running-mean filter.

complex processes include horizontal transport of air from different environments [Avallone and Prather, 1996; Selkirk et al., 2010].

### 3.2. Composite Seasonal Cycle

The soundings we have analyzed for this study are shown in Figure 4 in seasonal composite. Here we still show the trace gas concentration versus altitude; in subsequent figures we analyze the data in potential temperature coordinates. Figure 4 clearly shows the seasonal altitude shift of the TTL evident in Figure 1. During winter the potential temperature surfaces are shifted upward, lifting the ozone profile relative to summer. This is evident, for example, at the mean CP where the mean winter season ozone is 107 ppbv while it is 30 ppbv higher in summer. Water vapor is lower in the winter as well, but as we will argue later, this seasonal shift occurs at Costa Rica because the seasonal cycle of water vapor of the tropics is driven by dehydration in regions beyond Costa Rica, chiefly the western tropical Pacific.

The variation in the ozone and water concentration with height throughout the season is also evident in Figure 4, and this variation reflects the movement of the tropopause up and down as meteorological systems (waves) pass over Costa Rica as noted in Selkirk et al. [2010, Figure 7]. These results are consistent with the ozonesonde climatology produced by Logan [1999].

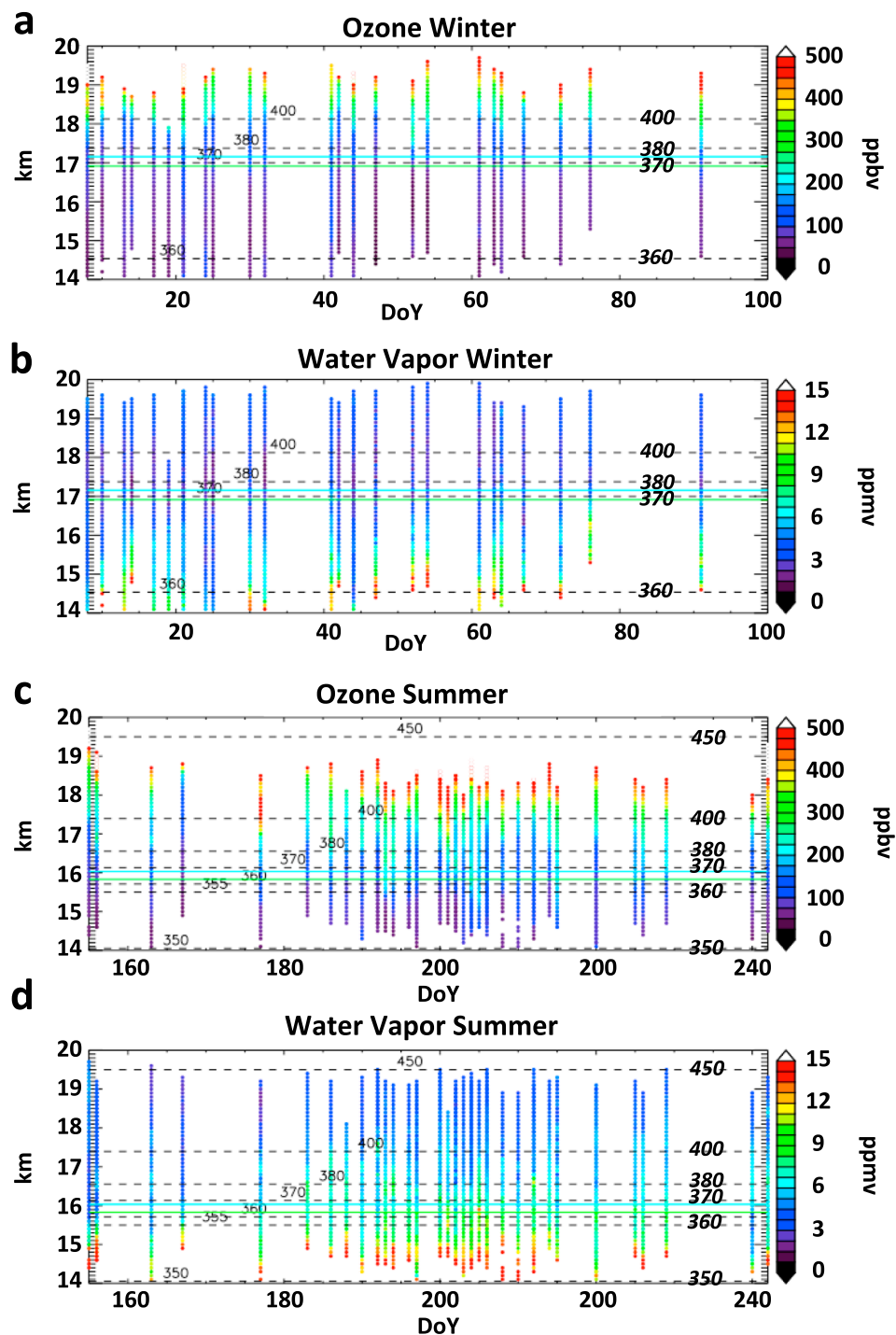
### 3.3. Seasonal Climatology in Potential Temperature Coordinates

Figure 5 composites the summer and winter ozone observations in potential temperature coordinates. Using potential temperature as the vertical coordinate reduces the effect of adiabatic systems shifting the profile up and down as seen in Figure 4. Even in potential temperature coordinates the sonde profiles for winter and summer are quite different. Ozone increases more rapidly with altitude in winter than in summer as seen in individual profiles in Figure 2. In the 370–380 K region, winter soundings are also drier by 2–3 ppmv and the tropopause is higher and colder than in summer. The use of potential temperature coordinates does not obviously remove all variability in water vapor and ozone, and higher water vapor values above 370 K tend to be visibly correlated with higher ozone.

The MLS v3.3 data were seasonally averaged over the 2005–2010 period, and the data were interpolated onto potential temperature surfaces using the MERRA reanalysis [Rienecker et al., 2011] and then to the location of Costa Rica. The average MLS water vapor profiles (Figures 5b and 5d) compare well with the sonde averages except at the lowest potential surfaces (360–370 K) where the MLS value is too low. These data at the bottom end of the MLS retrieval profile have high uncertainties, and the MLS averaging kernel will be dry biased by

The results are shown in Figure 3.  $F_\theta$  increases rapidly in the 3 km below the tropopause as the background ozone gradient increases.  $F_\theta$  peaks above the ozone tropopause where both the ozone gradient and wave variability are large, decreasing at higher altitudes as wave variability decreases. In the next section we will address the interrelationship between water vapor and ozone, but it is clear that significant negative excursions of water vapor tend to accompany positive anomalies of ozone and vice versa.

Although the Ticosonde data set does include a number of “typical” soundings, i.e., with ozone profiles lying close to the average profile, it is likely that the anomalous sonde profiles such as those shown in Figure 2 result from more complex processes than simple ascent and photochemistry of the typical profile as envisioned by Folkins et al. [2002]. Those



**Figure 4.** Seasonal composite sonde-measured composition versus altitude. (a, b) Boreal winter (December–February) profiles of ozone and water respectively with the color indicating the concentration of ozone (Figure 4a) or water vapor (Figure 4b). (c, d) Summer profiles (June–August). In Figures 4a and 4c the sonde is terminated when ozone exceeds 500 ppbv. Dashed lines show the seasonal average potential temperature surface altitudes.

the nonlinear increase in tropospheric water with decreasing altitude. The MLS ozone profile also shows higher values in the 360–390 K region where ozone is a few tens of parts per million by volume too high. Few studies provide validation of MLS ozone in this region, but a comparison of MLS and Umkehr data at the lowest levels is not inconsistent with this small high bias [Krzyscin et al., 2008].

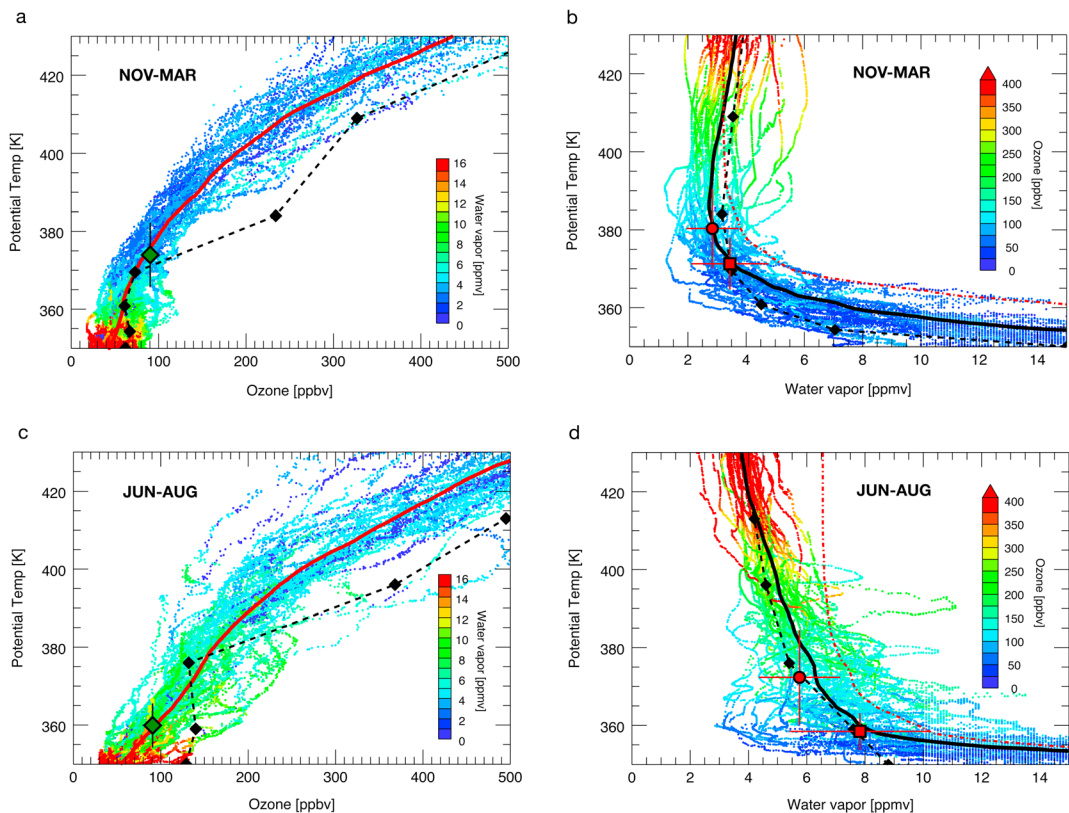


**Figure 5.** Ticosonde ozone and water vapor observations from (a, b) 38 winter and (c, d) 47 summer soundings versus potential temperature in Kelvin. Data points are color coded for water vapor mixing ratio (Figures 5a and 5c) and ozone mixing ratio (Figures 5b and 5d). Thick red (black) lines in each panel represent sonde seasonal average ozone (water vapor) mixing ratios. Symbols for the mean ozone tropopause (Figures 5a and 5c) and the mean CP and LRT (Figures 5b and 5d) are the same as in Figure 1. The dash-dotted red lines in Figures 5b and 5d define the local processing curve (see text). Mean MLS profiles are shown with black diamonds and dashed lines. MLS potential temperatures are computed from MERRA coincident meteorological data.

#### 4. Ozone and Water in the Tropical UT/LS

In the deep tropical UT/LS, where the net heating is positive—usually the region above 355–360 K in the tropics [Corti *et al.*, 2005; Fueglistaler and Fu, 2006]—and in the absence of convection, ozone is controlled by in situ production and upward vertical advection of lower concentration ozone from below [Folkins *et al.*, 2002]. In contrast to ozone, the water vapor mixing ratio is limited by the occurrence of supersaturation and subsequent ice removal by gravitational settling. Once dehydration is complete, the mixing ratio remains fixed as the air moves upward into the lower stratosphere until methane oxidation increases water above and outside the tropical lower stratosphere [Brewer, 1949; Gettelman and Forster, 2002; Jensen and Pfister, 2004; Fueglistaler *et al.*, 2005, 2009; Schoeberl and Dessler, 2011; Liu *et al.*, 2010; Schoeberl *et al.*, 2012].

In their analysis of Ticosonde data from campaigns in 2005 and 2007, Selkirk *et al.* [2010] note that the upper part of the TTL in summer was nearly always saturated (relative humidity (RH) > 100%) with respect to ice, and aircraft instruments show similar observations [Krämer *et al.*, 2009].

Ozone from the stratosphere might mix into the upper TTL, but in the TCSP and TC4 soundings this mixing rarely occurs below 350 K. Ice can be injected well into the UT/LS by overshooting convection where it can increase water concentration above its tropopause value [e.g., Hanisco *et al.*, 2007; Corti *et al.*, 2008], and this may be the case in some of the profiles contributing to Figure 5d. Convection can also loft tropospheric ozone into the TTL region decreasing the TTL ozone concentration expected from an advection-production model [Ziemke *et al.*, 2009].

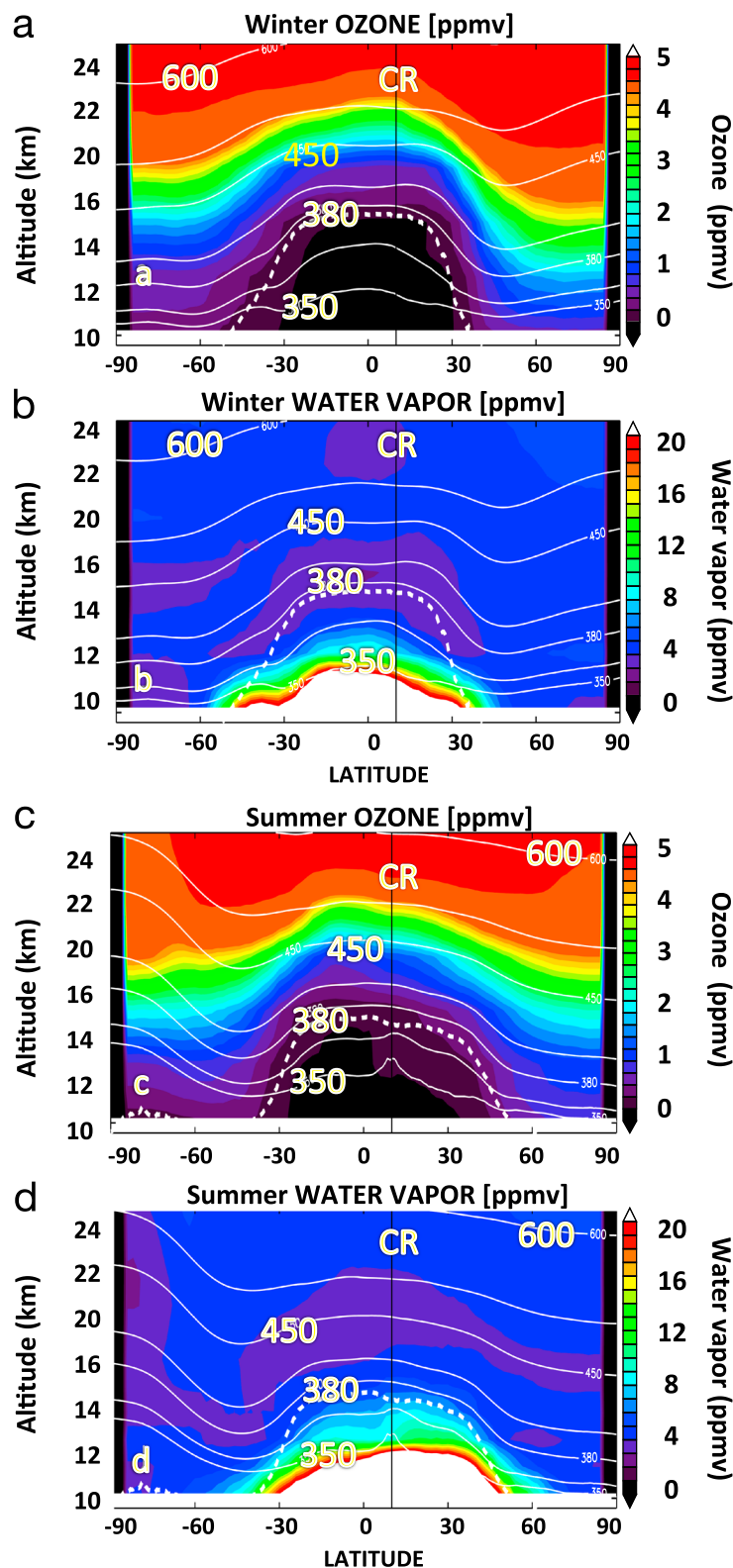


**Figure 6.** Five year average (2005–2010) MLS summer and winter observations at the longitude of San José, Costa Rica. Color scale on right. Note that the ozone scale extends linearly from 0 to 2 in 0.2 ppmv increments and then steps to 4 ppmv in 1 ppmv increments. White lines show the time-averaged potential temperature surfaces from 2008 to 2010 at the San José longitude; thick dashed line is the time-averaged zonal mean tropopause. Vertical black line shows the latitude of San José. (a) Winter ozone and (b) water vapor and (c) summer ozone and (d) water vapor.

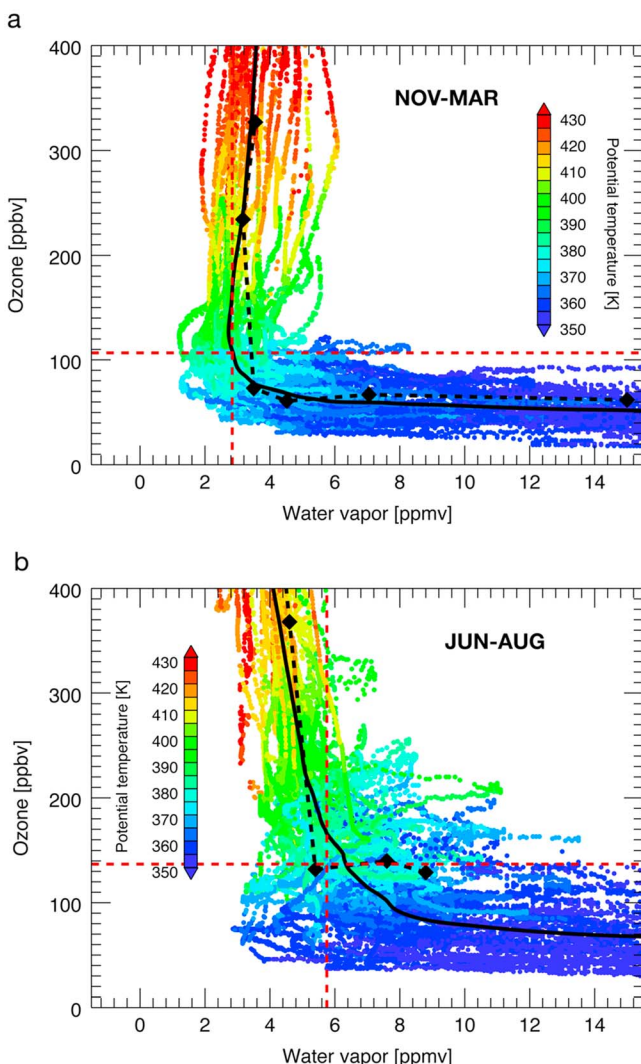


**Figure 7.** Ozone-water vapor scatterplots for (a) winter and (b) summer sonde ensembles. Dots are individual measurements color coded by potential temperature. The thick solid line is the average ozone for each water vapor value shown on the abscissa. The dashed red lines denote the ensemble CP tropopause for winter and summer, respectively. Black diamonds denote MLS data points from Figure 5.

popause is colder than the tropopause over San José [Hasebe et al., 2012, and references therein], and advection of this drier air would explain the observations.

In addition to advection from the TWP region, the ozone profiles for flights SJ055, SJ012, and SJ146 (Figures 2a, 2c, and 2d) suggest advection of ozone into the UT/LS from midlatitudes. To demonstrate that such transport is possible, Figure 6 shows the summer and winter MLS ozone and water vapor 5 year averages at the longitude of San José and the zonal mean tropopause. The isentropes above 350 K (averages of MERRA data for the period 2009–2010) clearly connect the tropics and midlatitudes, so it is possible for midlatitude ozone to move into the tropical region isentropically. This movement can explain the UT/LS layers of enriched ozone shown in Figures 2 and 5.

Plotting ozone against water gives further insight into the processes that can generate anomalies in the tropical trace gas profiles. Figure 7 shows ozone-water vapor plots for winter and summer with the points color coded for the potential temperature. Ozone in this case is a surrogate for the vertical coordinate. We show both sonde and MLS data in the figure. In the case of winter (Figure 7a), both the average sonde profiles and MLS data show a relatively sharp transition between the troposphere and the stratosphere in water vapor. (The dashed and dash-dotted lines in the figure show average ozone and water vapor at the CP—note

#### 4.1. Nonlocal Processes

Consideration of local processes (convection, dehydration, and mixing) neglects the impact of horizontal advection of air from different regions along potential temperature surfaces. The fact that water vapor cannot entirely be controlled by the local tropopause temperature is demonstrated in Figure 5 with the “local processing” water vapor profile. To compute the local processing, we imagine air parcels ascending vertically over Costa Rica and not exceeding 100% RH over ice as defined by Murphy and Koop [2005] and the sonde temperature and pressure. Of course, the air could be wetter than the 100% RH value when supersaturation occurs without cloud formation [Jensen et al., 2013]. Once the minimum water vapor saturation mixing ratio is reached, the profile above that point is fixed to the minimum value encountered. If air is simply slowly ascending, the minimum water vapor value is as dry as air can achieve using local sonde ascent pressures and temperatures. Averaging these profiles together, we obtain the local processing curve shown in Figure 5. Air ascending over San José cannot be drier than local processing curve; however, in both winter and summer, the water vapor concentration is lower than the local processing curve, proving that dehydration must have occurred elsewhere.

The TWP tropopause is colder than the tropopause over San José [Hasebe et al., 2012, and references therein], and advection of this drier air would explain the observations.

**Table 4.** Tropical Ozone/Water Measurements in the UT/LS

Season	Ozone	Water	
		H <sub>2</sub> O < 5 ppmv	H <sub>2</sub> O > 5 ppmv
Winter	O <sub>3</sub> < 90 ppbv	Dry air possibly from TWP	Upper tropospheric air not encountering the TWP or lower TTL air
	O <sub>3</sub> > 90 ppbv	In the stratosphere, air from TWP that has ascended to higher stratospheric altitudes (previous year's tape recorder signal)	In the troposphere, extratropical stratospheric air advected into the tropics
Summer	O <sub>3</sub> < 120 ppbv (TTL)	Air normally dehydrated near the tropopause (3 < H <sub>2</sub> O < 6 ppmv)	Upper tropospheric air-lower TTL
	O <sub>3</sub> > 120 ppbv	In the stratosphere, extratropical stratospheric air advected into the tropics	In the stratosphere, convectively moistened stratospheric air

that the transitional behavior in water occurs above 100 ppmv of ozone.) Within this sharp transition most water vapor data points vary between 1.5 and 6 ppmv. Both the variations below 3 ppmv and above 5 ppmv can be explained by advection of air to the sonde measurement point. For example, the coldest tropopause region is the TWP, but dehydration occurs in relatively warmer regions as well [Schoeberl and Dessler, 2011] which can explain the spread in the observed water vapor observations below  $\sim$ 3 ppmv. Evidence of midlatitude intrusions into the tropics is indicated by water values above  $\sim$ 3 ppmv. Midlatitude water vapor amounts are 4–5 ppmv on the same isentrope (Figure 6). Of course, tropical convective injection of water might account for water vapor amounts greater than  $\sim$ 3 ppmv, but a systematic contribution by convection seems unlikely since the higher water vapor is rarely found at potential temperature levels well above the maximum altitude of convective influence ( $\sim$ 390 K) [Zipser *et al.*, 2006; Dessler *et al.*, 2006] and the ozone values are clearly stratospheric. Note that occasionally, convective influence reaches much higher [Anderson *et al.*, 2012] in the summer outside the tropics.

The summer sonde data (Figure 7b) are strikingly different from the winter data. As noted above, the mean water vapor mixing ratio is higher for a given potential temperature and ozone values are lower (also see Figure 6). The scatter around the mean is higher in summer than in winter. Water vapor anomalies range from 8 to 10 ppmv for relatively high ozone values suggesting convective injection of ice that mixes with lower stratospheric air as has been observed [Hanisco *et al.*, 2007; Corti *et al.*, 2008]. Lateral mixing of air into the tropics from the extratropics can also explain anomalous summer ozone enhancements below 350 K.

Table 4 summarizes possible explanations for the sonde observations discussed above. Extratropical air is generally characterized by high ozone amounts and water vapor values between 4 and 6 ppmv; convectively moistened air will have higher water vapor values. In contrast, TWP air is very low in water and may have high ozone if it is air that is part of the previous winter's tape recorder signal.

#### 4.2. Stratosphere-Troposphere Exchange

In tracer-tracer diagrams, the presence of an L-shaped curve as seen in Figure 7 is evidence of a sharp transition at the tropopause. Pan *et al.* [2004, 2014] provided evidence that the change in the L of a sloping curve occurs in the presence of mixing at the tropopause. They noted that the region of sharpest transition (reduced mixing) occurred at high latitudes away from the subtropical jet. Likewise, Figure 7a suggests little exchange of air at the winter tropopause over Costa Rica. During this time of year Costa Rica is south of the subtropical jet. Air moving isentropically from the tropics to the midlatitudes, or the reverse, travels from the tropical upper troposphere to the midlatitude stratosphere. Pan *et al.* [2004, 2014] noted that cross-tropopause exchange can be quite efficient where the potential temperature surfaces are more orthogonal to the tropopause, namely, the region near the tropopause break. In that region, mixing of midlatitude air into the tropics can enhance ozone and water vapor in the upper tropical troposphere. Such mixing weakens the sharpness of the L shape seen in Figure 7b. The sharpness of the L shape of the winter curve suggests that there is little mixing between the tropical regions near San José and midlatitudes. This is consistent with the dynamical evidence for a mixing barrier between the tropics and midlatitudes in winter [e.g., Bowman and Hu, 1997; Haynes and Shuckburgh, 2000; Allen and Nakamura, 2001]. On the other hand, the curved tracer-tracer relationship in Figure 7b suggests a greater exchange of air between the tropical upper troposphere and midlatitude lowermost stratosphere during summer due to the weak mixing barrier.

#### 4.3. Sonde Back Trajectories

Above we hypothesized that anomalous parcels in different ozone-water vapor quadrants in Table 4 had different regional sources. To test this idea, we compute 5 day back trajectories from San José for JJA 2007

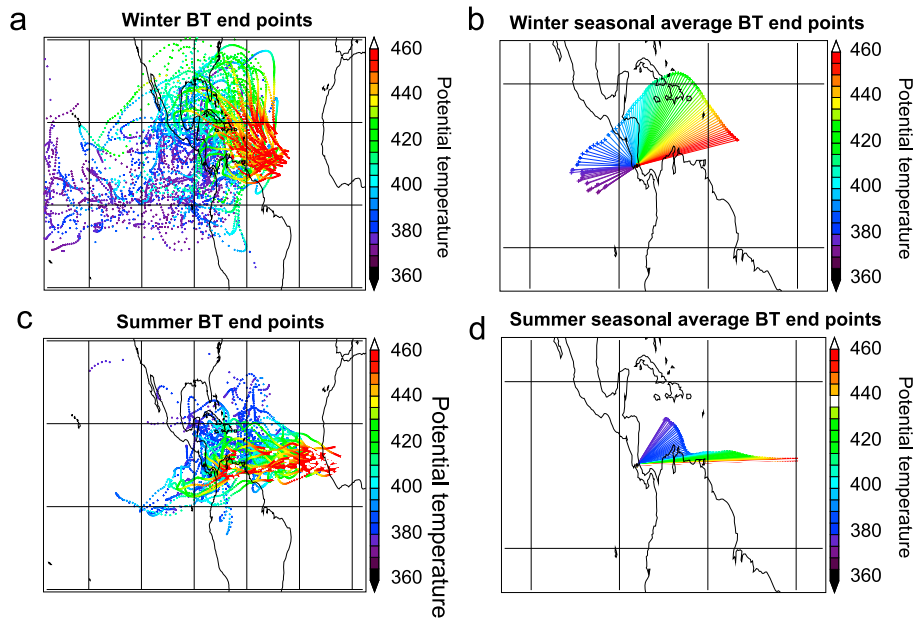


**Figure 8.** (a) End points of 5 day isentropic back trajectories initiated every 1 K from 350 to 450 K and for each day from San José, Costa Rica, in the period December 2006 to February 2007. (b) Seasonal average end points in Figure 8a at each PT level with a line connected to San José. (c) Same as Figure 8a but for June–August 2007 and (d) same as Figure 8b but for June–August 2007. The latitude-longitude grids are spaced 20° apart.

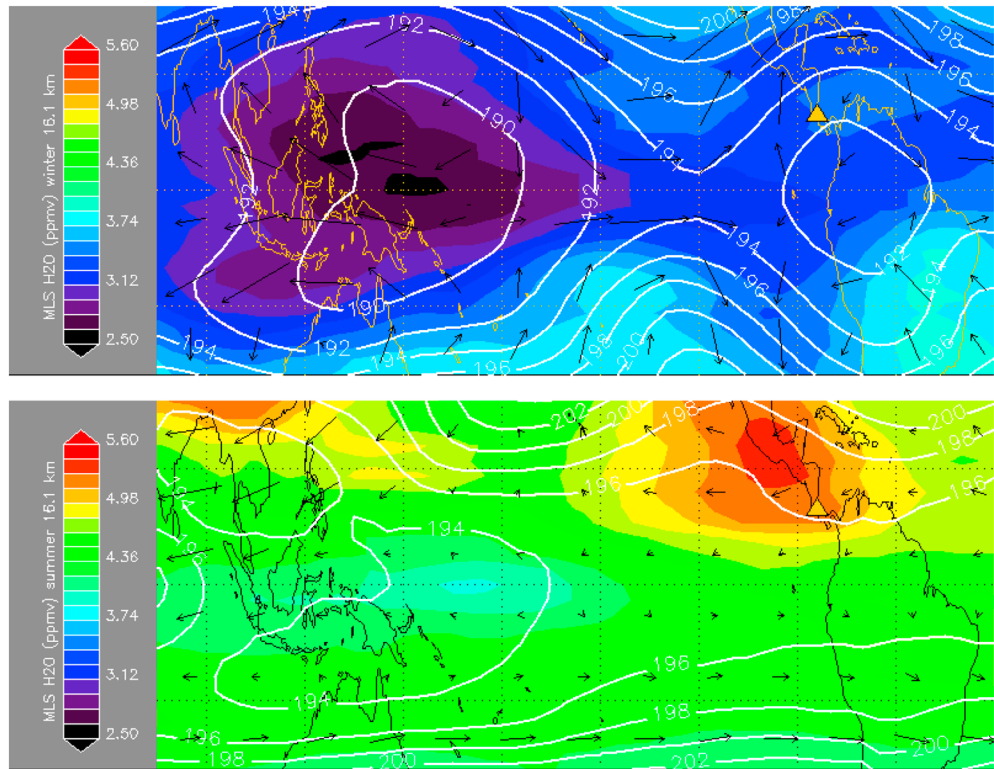


**Figure 9.** (top) DJF average water vapor field from MLS at 100 hPa (~16 km) with GEOS-5 winds overlaid. Triangle shows location of Costa Rica. White contours show the temperature. (bottom) JJA water vapor and wind fields at the same pressure level.

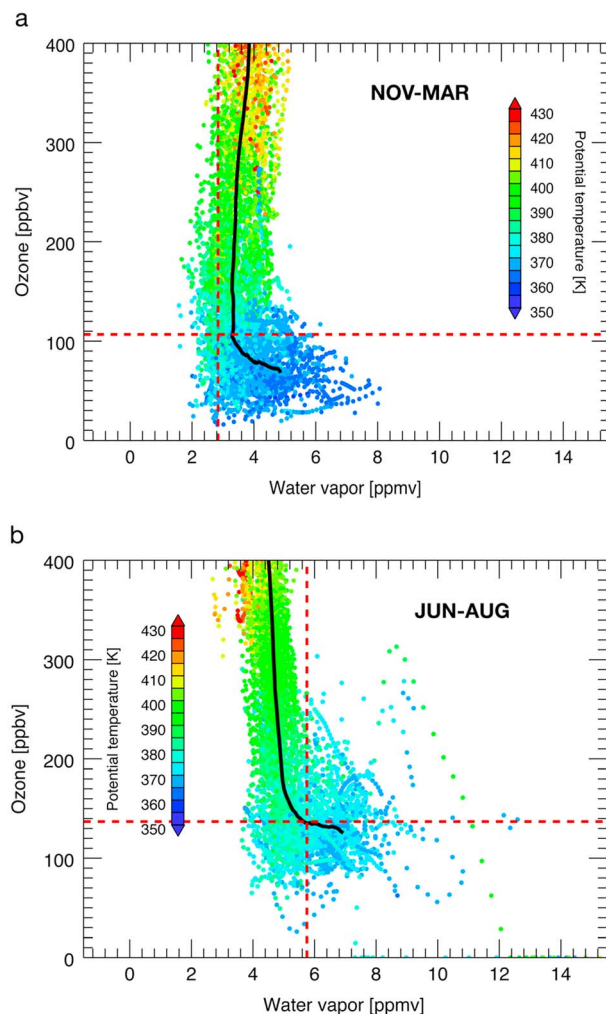


**Figure 10.** Results from a 5 day RDF calculation using MLS observations interpolated to the end points of the trajectories shown in Figure 8 for (a) winter and (b) summer. Mean profile is shown in heavy black line and dashed red lines as in Figure 7.

along with average wind field to support our interpretation that air moving into San José region is coming from the west and south as the back trajectories in Figures 8a and 8b indicate. Furthermore, air from this domain has water vapor values below 5 ppmv.

In the case of summer, parcels below the tropopause originate to northeast as the mean winds in JJA (Figure 9 (bottom)) demonstrate. Above the tropopause they mostly originate east of San José (Figures 8a and 8b). With the possibility of strong convective systems to the east during this season, air may be moistened even above the mean tropopause producing a high degree of variability in the UT/LS. This moistening could produce the excessive scatter in the ozone-water vapor diagram, Figure 7b.

#### 4.4. Simulation of Ticosonde Data Using Reverse Domain Filling

Using the back trajectories shown in Figure 8, we can perform reverse domain filling (RDF) calculations using MLS data to simulate sonde profiles. The RDF technique as applied to a horizontal field is discussed in Newman and Schoeberl [1995]; in this case it is applied to a vertical profile. The RDF method is as follows: a regular grid is laid down, and back trajectories are used to locate origin points on the grid. In the case of trace gases, the mixing ratio is brought forward in time along the trajectory path to the grid point. The RDF technique creates more structure as wind shear sharpens gradients. To apply the RDF technique, in this case

and December-January-February (DJF) (2006–2007). Longer trajectories are more uncertain, especially in the tropics. Figure 8 shows the termini for each day as well as the time-mean positions of 5 day isentropic back trajectories. Each point is colored by potential temperature. The back trajectories are computed using the MERRA reanalysis.

In the case of winter (Figures 8a and 8b) parcels at potential temperatures below the CP tropopause originate primarily to the west of San José while the parcels in the lower stratosphere originate to the north and to the east. This supports the idea that the upper troposphere parcels will have been dehydrated in the TWP (to the west), giving rise to the very low values of water vapor seen in Figure 7a for ozone amounts  $< 90$  ppbv. Above the tropopause, the air on average originates northeast of Costa Rica and at even higher potential temperatures to the east. Air coming from the northeast and east will have the signature of the previous summer ozone and water vapor amounts explaining the increase in water above the tropopause levels. Strong convection is rare in the Gulf of Mexico during this period; Figure 7 shows evidence of little convective moistening of the lower stratospheric air as expected. We show the long-term average MLS water vapor field for the winter season at 100 in Figure 9 (top)

and December-January-February (DJF) (2006–2007).

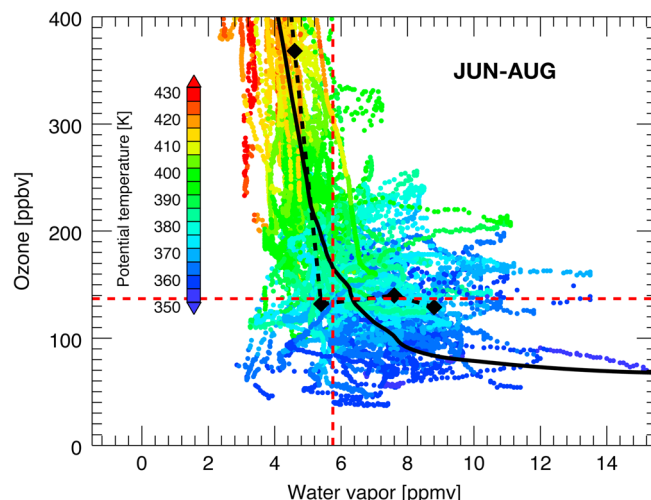


**Figure 11.** Same as Figure 7b except that all points below the lapse rate tropopause are eliminated.

as sharp in the RDF calculation due to the lower vertical resolution of the MLS data compared to sondes. The stratospheric MLS mean over Costa Rica shown in Figure 7 is comparable to the RDF mean in Figure 10a. The tropospheric mean water is lower in the RDF for comparable ozone values than the MLS climatology over Costa Rica. We attribute this to the higher uncertainty of MLS water retrievals within the upper troposphere.

The differences in the summer data are much more informative (Figures 7b and 10b). While the RDF and sonde data agree in the region where ozone values  $>150$  ppbv, there are many more high water vapor sonde observations for typical UT/LS ozone values than seen in the RDF. This discrepancy may be explained by the addition of water along the 5 day parcel path between the time it is observed by MLS and the time it is observed by the sonde, or by stratospheric ozone being injected into the troposphere along isentropes and mixed with the higher water amounts in the lower TTL. To distinguish the two mechanisms, we can eliminate data below the tropopause; this removes the possibility of stratospheric ozone injection. Figure 11 shows the summer Ticosonde results after removing all data below the WMO tropopause. The results are very similar to Figure 7b leading us to conclude that the predominant source of variability in stratospheric water vapor over Costa Rica is the injection of water into the stratosphere through convective events.

## 5. Discussion

Our analysis of Ticosonde data extends the previous studies by Selkirk *et al.* [2010] and Fujiwara *et al.* [2010]. Balloonsonde profiles of water vapor and ozone made in Costa Rica (2005–2011) show three reasons for intersonde variability in the UT/LS: wave-induced vertical motion across strong vertical gradients (wave variability) as noted in Selkirk *et al.* [2010, Figure 7], differences in source air masses (e.g., TWP or midlatitudes) resulting from horizontal transport (source variability), and changes induced along parcel paths due to physical and/or chemical processes (path variability). Of course, if the backward path is long enough, path variability and source variability become indistinguishable. In comparing individual sonde profiles, wave variability is the largest source of differences (see Figures 1 and 2). Wave variability can be reduced by (1) compositing the soundings with respect to the tropopause [e.g., Logan, 1999] or (2) compositing soundings relative to potential temperature (Figure 3) [Selkirk *et al.*, 2010], (3) using ozone as a vertical coordinate—making an ozone/water diagram (Figure 5).

In the case of water vapor, both convective injection and cloud dehydration are causes of path variability and can give rise to anomalies in ozone-water diagrams. The lack of a mixing barrier dividing the tropics from midlatitudes in summer allows midlatitude air to penetrate the tropics—at least at the lowest potential temperatures in summer (Figure 8b). In addition, convective injection of water (as suggested in Figure 11) may also occur along the westward path of air parcels moving toward Costa Rica (Figures 8b and 9). Using lightning as a surrogate for storm intensity (and cloud tops), Christian *et al.* [2003] report that the region

we take MLS observations interpolated to the trajectory end points shown in Figure 8. The spatial change in vertical water and ozone gradients produces structure in the vertical RDF. The ozone-water vapor plot that results is shown in Figure 10, and this plot should be compared to Figure 7 which shows sonde ozone and water vapor averages and MLS data over Costa Rica.

First, comparing winter periods (Figures 7a and 10a), the agreement is fairly good although there is a slight high bias ( $<0.5$  ppmv) in the stratospheric MLS water vapor RDF. This bias is within the range reported by Fujiwara *et al.* [2010] and the MLS accuracy [Livesey *et al.*, 2011]. As expected the L shape in the Ticosonde ozone-water diagram is not

around Venezuela produces significant convection in summer and the Venezuelan convective region is occasionally along the parcel paths leading toward San José.

During the winter, balloonsonde water vapor amounts are observed to be well below the saturation mixing ratios. Back trajectory analysis shows that this air has arrived from the west and has likely been dehydrated in the TWP or near that cold zone. The variance in water vapor observations suggests a variety of pathways through the TWP region.

## 6. Summary

Balloonsonde profiles of water vapor and ozone made at Costa Rica from 2005 to 2011 are analyzed by compositing the data for the summer and winter seasons in potential temperature coordinates and in ozone-water diagrams. We focus on data in the upper troposphere and lower stratosphere (UT/LS). We find that the summer and winter sonde climatologies are very different. In winter, water amounts are very low near the tropopause—much lower than expected from local ice saturation temperatures. Water decreases rapidly with potential temperature to the CP, then increases from there up to about 500 K, and then stays relatively constant to the upper limit of the sonde data (~700 K). In contrast, during summer water continues to decrease above the CP until reaching the previous winter's minimum mixing ratio. In addition, the summer water vapor sonde data show a much higher degree of water variability compared to winter. These differences are even more dramatic in ozone-water diagrams.

We describe three mechanisms that produce short-time variability between soundings: wave-induced vertical motion across strong vertical gradients (wave variability), differences in source air masses resulting from horizontal transport (source variability), and changes induced along parcel paths due to physical and/or chemical processes (path variability). Wave variability is responsible for most of the variation between sonde profiles within a given season. Summer to winter differences are caused by other factors. Source variability means that the air arrives from different regions, e.g., TWP or midlatitudes. Air from the midlatitude stratosphere can move isentropically into the tropics in summer when transport barriers are weak. The variety of source regions is reflected in the spread of 5 day back trajectory termini shown in Figure 8.

Path variability occurs when the air parcel is modified as it moves from the source region to the measurement point. In the case of water vapor, both convective injection and dehydration can occur along the path. Table 1 describes different sources of variability using the ozone-water relationship to describe different regimes. Finally, we further investigated the summer sonde variability using a vertical RDF with MLS data. Our results suggest that convective moistening of stratospheric air occurs in summer leading to more variability among summer sonde measurements and higher water in the stratosphere than might be expected.

## References

- Allen, D. R., and N. Nakamura (2001), A seasonal climatology of effective diffusivity in the stratosphere, *J. Geophys. Res.*, **106**, 7917–7935, doi:10.1029/2000JD900717.
- Anderson, J. G., D. Wilmouth, J. B. Smith, and D. S. Sayres (2012), UV dosage levels in summer: Increased risk of ozone loss from convectively injected water vapor, *Science*, **337**, 835–839.
- Avallone, L. M., and M. J. Prather (1996), Photochemical evolution of ozone in the lower tropical stratosphere, *J. Geophys. Res.*, **101**, 1457–1461.
- Bowman, K. P., and Y. Hu (1997), Tropical mixing barriers in the lower stratosphere in the Geophysical Fluid Dynamics Laboratory SKYHI model, *J. Geophys. Res.*, **102**, 21,465–21,478, doi:10.1029/97JD01606.
- Brewer, A. W. (1949), Evidence for a world circulation provided by the measurements of helium and water vapour distribution in the stratosphere, *Q. J. R. Meteorol. Soc.*, **75**, 351–363, doi:10.1002/qj.49707532603.
- Christian, H. J., et al. (2003), Global frequency and distribution of lightning as observed from space by the Optical Transient Detector, *J. Geophys. Res.*, **108**(D1), 4005, doi:10.1029/2002JD002347.
- Corti, T., B. P. Luo, T. Peter, H. Vömel, and Q. Fu (2005), Mean radiative energy balance and vertical mass fluxes in the equatorial upper troposphere and lower stratosphere, *Geophys. Res. Lett.*, **32**, L06802, doi:10.1029/2004GL021889.
- Corti, T., et al. (2008), Unprecedented evidence for deep convection hydrating the tropical stratosphere, *Geophys. Res. Lett.*, **35**, L10810, doi:10.1029/2008GL033641.
- Danielsen, E. F. (1982), A dehydration mechanism for the stratosphere, *Geophys. Res. Lett.*, **9**, 605–608, doi:10.1029/GL009i006p00605.
- Dessler, A. E., S. P. Palm, and J. D. Spinhirne (2006), Tropical cloud-top height distributions revealed by the Ice, Cloud, and Land Elevation Satellite (ICESat)/Geoscience Laser Altimeter System (GLAS), *J. Geophys. Res.*, **111**, D12215, doi:10.1029/2005JD006705.
- Folkins, I., M. Loewenstein, J. Podolske, S. J. Oltmans, and M. Proffitt (1999), A barrier to vertical mixing at 14 km in the tropics: Evidence from ozonesondes and aircraft measurements, *J. Geophys. Res.*, **104**, 22,095–22,102, doi:10.1029/1999JD900404.
- Folkins, I., C. Braun, A. Thompson, and J. Witte (2002), Tropical ozone as an indicator of deep convection, *J. Geophys. Res.*, **107**(D13), 4184, doi:10.1029/2001JD001178.

## Acknowledgments

The authors would like to acknowledge the dedicated efforts of the extended group who worked together to create the Ticosonde data set. This has included, among many others, Jessica Valverde, Werner Stoltz, Jorge Andrés Diaz, and Gary Morris; Walter Fernandez, Jorge Amador, and Eladio Zárate; Leonhard Pfister, Randy May, Grace S. Peng, Jimena Lopez, and Marion Legg; Victor Hugo Beita, Karla Cerna, Diana González, Jose Pablo Sibaja, Ilena Vega, Rosa Alfaro, and Sebastian Miranda; Juan Valdés, Victor Hernández, Kristel Heinrich, Marcial Garbanzo and Gustavo Garbanzo; and Ernesto Corrales, Yetty Madrigal, and Sara Azofeifa. We also acknowledge support from the following institutions in Costa Rica: Instituto Meteorológico Nacional, Universidad de Costa Rica, Universidad Nacional, and Comité Regional de Recursos Hidráulicos. M.R.S. would also like to acknowledge the use of the Texas A&M computers to perform the trajectory calculations. Finally, H.B.S. would like to thank Karen Rosenlof of the NOAA Earth Sciences Research Laboratory for the use of her lapse rate tropopause code. We would also like to thank the anonymous reviewers for their many helpful comments. This work was supported by NASA's Upper Atmosphere Research Program and the Radiation Sciences Program. The MLS data are available through <http://mls.jpl.nasa.gov>. Ticosonde sounding data are available through the Aura Validation Data Center (AVDC, <http://avdc.gsfc.nasa.gov>) at NASA Goddard Space Flight Center.

- Fueglistaler, S., and Q. Fu (2006), Impact of clouds on radiative heating rates in the tropical lower stratosphere, *J. Geophys. Res.*, **111**, D23202, doi:10.1029/2006JD007273.
- Fueglistaler, S., M. Bonazzola, P. H. Haynes, and T. Peter (2005), Stratospheric water vapor predicted from the Lagrangian temperature history of air entering the stratosphere in the tropics, *J. Geophys. Res.*, **110**, D08107, doi:10.1029/2004JD005516.
- Fueglistaler, S., A. E. Dessler, T. J. Dunkerton, I. Folkins, Q. Fu, and P. W. Mote (2009), Tropical tropopause layer, *Rev. Geophys.*, **47**, RG1004, doi:10.1029/2008RG000267.
- Fujiwara, M., et al. (2010), Seasonal to decadal variations of water vapor in the tropical lower stratosphere observed with balloon-borne cryogenic frost point hygrometers, *J. Geophys. Res.*, **115**, D18304, doi:10.1029/2010JD014179.
- Gettelman, A., and P. M. d. F. Forster (2002), A climatology of the tropical tropopause layer, *J. Meteorol. Soc. Jpn.*, **80**, 911–942.
- Hanisco, T. F., et al. (2007), Observations of deep convective influence on stratospheric water vapor and its isotopic composition, *Geophys. Res. Lett.*, **34**, L04814, doi:10.1029/2006GL027899.
- Hasebe, F., et al. (2012), Cold trap dehydration in the Tropical Tropopause Layer characterized by SOWER chilled-mirror hygrometer network data in the tropical Pacific, *Atmos. Chem. Phys. Discuss.*, **12**, 25,833–25,885, doi:10.5194/acpd-12-25833-2012.
- Haynes, P., and E. Shuckburgh (2000), Effective diffusivity as a diagnostic of atmospheric transport: 1. Stratosphere, *J. Geophys. Res.*, **105**, 22,777–22,794, doi:10.1029/2000JD900093.
- Holton, J. R., and A. Gettelman (2001), Horizontal transport and the dehydration of the stratosphere, *Geophys. Res. Lett.*, **28**, 2799–2802, doi:10.1029/2001GL013148.
- Jensen, E. J., and L. Pfister (2004), Transport and freeze-drying in the tropical tropopause layer, *J. Geophys. Res.*, **109**, D02207, doi:10.1029/2003JD004022.
- Jensen, E. J., G. Diskin, R. P. Lawson, S. Lance, T. P. Bui, D. Hlavka, M. McGill, L. Pfister, O. B. Toon, and R. S. Gao (2013), Ice nucleation and dehydration in the Tropical Tropopause Layer, *Proc. Natl. Acad. Sci. U.S.A.*, **110**, 2041–2046.
- Komhyr, W. D., R. A. Barnes, G. B. Brothers, J. A. Lathrop, and D. P. Opperman (1995), Electrochemical concentration cell ozonesonde performance evaluation during STOIC 1989, *J. Geophys. Res.*, **100**, 9231–9244, doi:10.1029/94JD02175.
- Krämer, M., et al. (2009), Ice supersaturations and cirrus cloud crystal numbers, *Atmos. Chem. Phys.*, **9**, 3505–3522.
- Krzyscik, J. W., J. Jaroslawski, B. Rajewska-Wiech, P. S. Sobolewski, and L. Froidevaux (2008), Comparison of ozone profiles by the Umkehr measurements taken at Belsk (52°N, 21°E) with the Aura Microwave Limb Sounder overpasses: 2004–2006, *J. Geophys. Res.*, **113**, D15S09, doi:10.1029/2007JD008586.
- Liu, Y. S., S. Fueglistaler, and P. Haynes (2010), Advection-condensation paradigm for stratospheric water vapor, *J. Geophys. Res.*, **115**, D24307, doi:10.1029/2010JD014352.
- Livesey, N., et al. (2011), EOS MLS version 3.3 level 2 data quality and description document, *Tech. Rep. JPK D-33509*, Jet Propul. Lab., Calif. Inst. Technol., Pasadena, Calif.
- Logan, J. A. (1999), An analysis of ozonesonde data for the troposphere: Recommendations for testing 3-D models and development of a gridded climatology for tropospheric ozone, *J. Geophys. Res.*, **104**, 16,115–16,149, doi:10.1029/1998JD100096.
- Mote, P. W., K. H. Rosenlof, M. E. McIntyre, E. S. Carr, J. C. Gille, J. R. Holton, J. S. Kinnersley, H. C. Pumphrey, J. M. Russell III, and J. W. Waters (1996), An atmospheric tape recorder: The imprint of tropical tropopause temperatures on stratospheric water vapor, *J. Geophys. Res.*, **101**, 3989–4006, doi:10.1029/95JD03422.
- Murphy, D. M., and T. Koop (2005), Review of the vapour pressures of ice and supercooled water for atmospheric applications, *Q. J. R. Meteorol. Soc.*, **131**, 1539–1565.
- Newell, R. E., and S. Gould-Stewart (1981), A stratospheric fountain?, *J. Atmos. Sci.*, **38**, 2789–2796.
- Newman, P. A., and M. R. Schoeberl (1995), A reinterpretation of the data from the NASA Stratosphere-Troposphere Exchange Project, *Geophys. Res. Lett.*, **22**, 2501–2504, doi:10.1029/95GL02220.
- Pan, L. L., W. J. Randel, B. L. Gary, M. J. Mahoney, and E. J. Hintsa (2004), Definitions and sharpness of the extratropical tropopause: A trace gas perspective, *J. Geophys. Res.*, **109**, D23103, doi:10.1029/2004JD004982.
- Pan, L. L., L. C. Paulik, S. B. Honomichl, L. A. Munchak, J. Bian, H. B. Selkirk, and H. Vömel (2014), Identification of the tropical tropopause transition layer using the ozone-water vapor relationship, *J. Geophys. Res. Atmos.*, **119**, 3586–3599, doi:10.1002/2013JD020558.
- Peter, T., C. Marcolla, P. Spichtinger, T. Corti, M. B. Baker, and T. Koop (2006), When dry air is too humid, *Science*, **314**(5804), 1399–1402.
- Prather, M. J., X. Zhu, Q. Tang, J. Hsu, and J. L. Neu (2011), An atmospheric chemist in search of the tropopause, *J. Geophys. Res.*, **116**, D04306, doi:10.1029/2010JD014939.
- Randel, W. J., and E. J. Jensen (2013), Physical processes in the tropical tropopause and their roles in a changing climate, *Nat. Geosci.*, **6**, 169–176.
- Randel, W. J., M. Park, F. Wu, and N. Livesey (2007), A large annual cycle in ozone above the tropical tropopause linked to the Brewer-Dobson circulation, *J. Atmos. Sci.*, **64**, 4479–4488.
- Rienecker, M., et al. (2011), MERRA: NASA's Modern-Era Retrospective Analysis for Research and Applications, *J. Clim.*, **24**, 3624–3648, doi:10.1175/JCLI-D-11-00015.1.
- Schoeberl, M. R., and A. E. Dessler (2011), Dehydration of the stratosphere, *Atmos. Chem. Phys.*, **11**, 8433–8446.
- Schoeberl, M. R., A. E. Dessler, and T. Wang (2012), Simulation of stratospheric water vapor and trends using three reanalyses, *Atmos. Chem. Phys.*, **12**, 6475–6487.
- Selkirk, H. B., H. Vömel, J. M. Valverde Canossa, L. Pfister, J. A. Diaz, W. Fernández, J. Amador, W. Stoltz, and G. S. Peng (2010), Detailed structure of the tropical upper troposphere and lower stratosphere as revealed by balloon sonde observations of water vapor, ozone, temperature, and winds during the NASA TCSP and TC4 campaigns, *J. Geophys. Res.*, **115**, D00J19, doi:10.1029/2009JD013209.
- Sherwood, S. C., and A. E. Dessler (2003), Convective mixing near the tropical tropopause: Insights from seasonal variations, *J. Atmos. Sci.*, **60**, 2674–2685.
- Stolarski, R. S., D. W. Waugh, L. Wang, L. D. Oman, A. R. Douglass, and P. A. Newman (2014), Seasonal variation of ozone in the tropical lower stratosphere: Southern tropics are different from northern tropics, *J. Geophys. Res. Atmos.*, **119**, 6196–6206, doi:10.1002/2013JD021294.
- Vömel, H., et al. (2002), Balloon-borne observations of water vapor and ozone in the tropical upper troposphere and lower stratosphere, *J. Geophys. Res.*, **107**(D14), 4210, doi:10.1029/2001JD000707.
- Vömel, H., D. E. David, and K. Smith (2007), Accuracy of tropospheric and stratospheric water vapor measurements by the cryogenic frost point hygrometer: Instrumental details and observations, *J. Geophys. Res.*, **112**, D08305, doi:10.1029/2006JD007224.
- Ziemke, J. R., J. Joiner, S. Chandra, P. K. Bhartia, A. Vasilkov, D. P. Haffner, K. Yang, M. R. Schoeberl, L. Froidevaux, and P. F. Levelt (2009), Ozone mixing ratios inside tropical deep convective clouds from OMI satellite measurements, *Atmos. Chem. Phys.*, **9**, 573–583, doi:10.5194/acp-9-573-2009.
- Zipser, E. J., D. J. Cecil, C. Liu, S. W. Nesbitt, and D. P. Yorty (2006), Where are the most intense thunderstorms on Earth?, *Bull. Am. Meteorol. Soc.*, **87**, 1057–1071.